ADVANCED FUNCTIONAL MATERIALS
www.afm-journal.de

Rolling Friction Enhanced Free-Standing Triboelectric Nanogenerators and their Applications in Self-Powered Electrochemical Recovery Systems

*Min-Hsin Yeh, Hengyu Guo, Long Lin, Zhen Wen, Zhaoling Li, Chenguo Hu, and Zhong Lin Wang**

Heavy metals contained in wastewater are one of the most serious pollutions in natural resources. A self-powered electrochemical recovery system for collecting Cu ions in wastewater by incorporating a rolling friction enhanced freestanding triboelectric nanogenerator (RF-TENG) is developed here. The RF-TENG utilizes integrated cylindrical surfaces using the conjunction of rolling electrification and freestanding electrostatic induction, which shows outstanding output performance and ultrarobust stability. By using the kinetic energy of flowing water, a collection efficiency of up to 80% for Cu^{2+} ions in wastewater has been achieved. Self-powered electrochemical systems are one of the most promising applications of TENGs for independent and sustainable driving of electrochemical reactions without the need for any additional power supply. This research is a substantial advancement towards the practical applications of triboelectric nanogenerators and self-powered electrochemical systems.

1. Introduction

Industrial wastewater is produced as a by-product to many industrial processes and containing several types of toxic chemical compounds (e.g., acid cyanide and alkaline-based agents) and heavy metal ions (e.g., Cu, Ni, and Cr).[1] Most of the heavy metals in wastewater are extremely harmful if they are directly discharged into the sewer without any treatment, because of their high solubility in aquatic environments and their high absorption by living organisms. Once these heavy metals enter into our food chain, large concentrations of heavy metals may be accumulated in the human body and may induce severe illness. Hence, providing an efficient industrial wastewater treatment for removing or collecting these heavy metals before discharging has become an important and necessary tool. Copper (Cu) is one of the most common heavy metal ions in wastewater, resulting among others from printed circuit board (PCB) processes. Several approaches have been proposed for Cu removal from industrial wastewater, such as chemical precipitation, adsorption, and ion exchange.[2] One of the most effective ways for collecting Cu ions is the electrodeposition process.[3] A plate-electrode-based electrochemical process has been shown to be an efficient method to remove Cu ions from dilute industrial effluent. Moreover, Cu is deposited in an extremely high quality (>99%), which can then be collected from the surface of the electrode without any further purification process. However, to be able to realize the above electrochemical process, an additional direct current (DC) based power supply is indispensable to keep it working.

Recently, self-powered systems have been proposed and developed to integrate into several systems for sensing, communication, computation, and so on.[4] The large number of miniaturized components in electronic systems require a renewable and sustainable power supply. In such cases, being able to harvest the energy from the ambient environment would be a reasonable solution for this problem. Based on the coupling effect of contact electrification and electrostatic induction, triboelectric nanogenerators (TENGs) have recently been shown to be renewable and sustainable power generators for converting ambient mechanical energy into electricity.[5] In the past few years, the output power density of TENGs has been drastically increased through several advanced material optimizations and structural design adaptations.[6] Moreover, compared to conventional electromagnetic generators (EMGs), TENGs have the advantages of simple fabrication, reasonable robustness, and low cost, indicating their higher potential for integration with other functional devices for practical applications.[7] By incorporating TENGs as the power supply, various types of self-powered systems have been successfully realized, such as wireless sensor networks,[8] electrochemical reactions,[9]

Dr. M.-H. Yeh, H. Guo, Dr. L. Lin, Z. Wen, Z. Li, Prof. Z. L. Wang
School of Materials Science and Engineering
Georgia Institute of Technology
Atlanta, Georgia 30332–0245, USA
E-mail: zlwang@gatech.edu
H. Guo, Prof. C. Hu
Department of Applied Physics
Chongqing University
Chongqing 400044, P. R. China
Prof. Z. L. Wang
Beijing Institute of Nanoenergy and Nanosystems
Chinese Academy of Sciences
Beijing 100083, P. R. China

DOI: 10.1002/adfm.201504396

chemical sensors,[10] etc. To realize practical and commercial applications of these self-powered systems, it is highly desirable that the output of TENGs can be converted into a constant DC output with high current.

In this work, a rolling friction enhanced free-standing triboelectric nanogenerator (RF-TENG) is presented in a parallel cylindrical structure, which shows a high output performance and ultra-robust stability. The predicament of static charge dissipation in the free-standing TENG was well resolved without compromising the device robustness by utilizing the rolling friction from a metal rod.[11] The rolling rod continuously replenished the tribo-charges in the free-standing triboelectric layer to a saturated level. This replenishment assured a high electric output, while the rolling friction caused almost no damage to the triboelectric layers. The energy harvested from flowing water by the RF-TENG was applied to a self-powered electrochemical recovery system for collecting Cu ions from wastewater. Using the above design, the RF-TENG delivered an open-circuit voltage (V_{OC}) of up to 650 V and a short-circuit current (I_{SC}) of 280 μA at a rotation speed of 1500 rpm. The ultra-robustness could be realized by introducing a frictionless free-standing structure with a rolling bearing for refilling its superficial charge. Moreover, several units of this RF-TENG could easily be put together by incorporating mechanical gears to form an integrated RF-TENG bundled structure. Using a transformer and a power management circuit, a stable DC output (5 V, 4 mA) was achieved by the water-flow driven RF-TENG that realized the concept of a self-powered electrochemical recovery system for collecting Cu ions. Moreover, several other electrochemical processes for practical wastewater electrochemical treatments, such as electrocoagulation, electroflotation, electrochemical degradation, and electrochemical advanced oxidation process, could also be driven by our proposed self-powered electrochemical processor. This work provides a significant progress in TENG fabrication and exhibits huge potential of the RF-TENG as a high efficiency energy harvester for practical applications.

2. Results and Discussion

The integrated power generation device was assembled using several individual units of the RF-TENG. The output performance from all these units could be synchronized by choosing an appropriate gearing and bearing system. The rotors were driven to make a relative rotation motion against the stators. To obtain a better understanding of its working principle, the structural design of a single RF-TENG unit, which consists of a rotor, a stator, and a shaft, is illustrated in **Figure 1**a. In the rotor, a layer of parallel copper stripes was uniformly deposited onto the fluorinated ethylene propylene (FEP) thin film and then wrapped onto the soft-sponge-coated acrylic rod. The soft sponge foam acted as a buffer layer to assure an intimate contact between the surfaces of the shaft and the rotor. The enlarged illustration shows the function of the copper shaft for charge replenishment via rolling electrification with the surface of the rotor. A Kapton film with deposited copper interdigitated electrode was attached to the inner plane of the

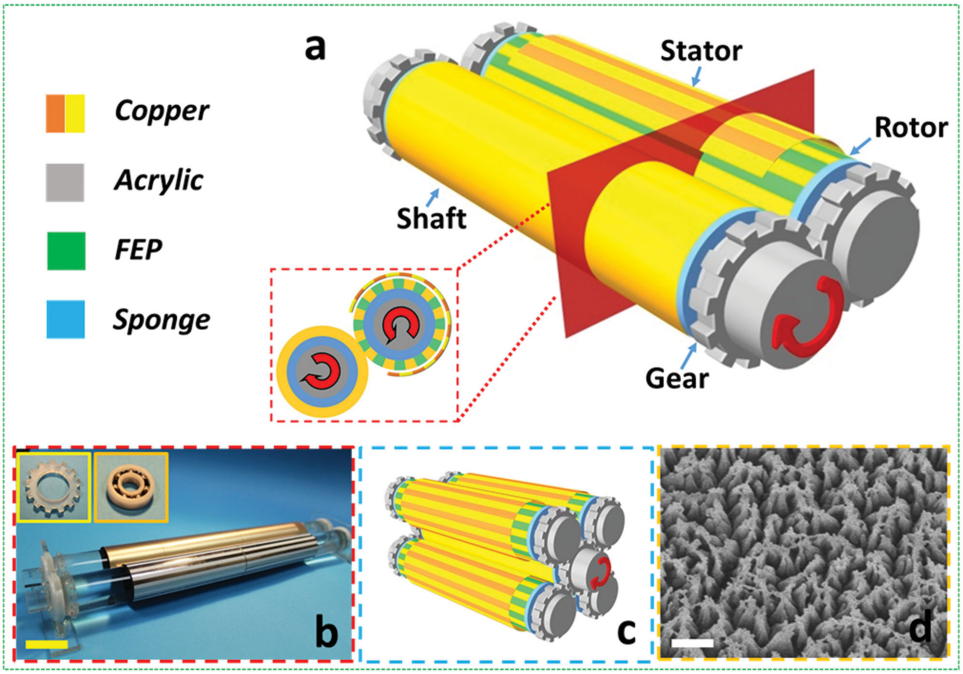

Figure 1. Structural design of the cylindrical rod structure of a rolling friction enhanced free-standing triboelectric nanogenerator (RF-TENG). a) Schematic illustration of the RF-TENG unit. The zoomed-in illustration demonstrates the functionality of the copper shaft for charge replenishment via rolling friction. b) Photograph of a connected shaft/rotor unit linked by gears. A Cu foil covered acrylic rod and acrylic rod coated with Cu gratings patterned FEP film were utilized as the shaft and rotor, respectively. A mechanical gear (left) and a bearing (right) are shown as the inset. The scale bar is 1 cm. c) Schematic illustration of the RF-TENG device, which consisted of a Cu foil covered acrylic rod as a shaft, and four RF-TENGs units each comprising a rotor and a stator. d) SEM image of the FEP film with the nanowires array structure. The scale bar is 500 nm.

Adv. Funct. Mater. **2015**,
DOI: 10.1002/adfm.201504396

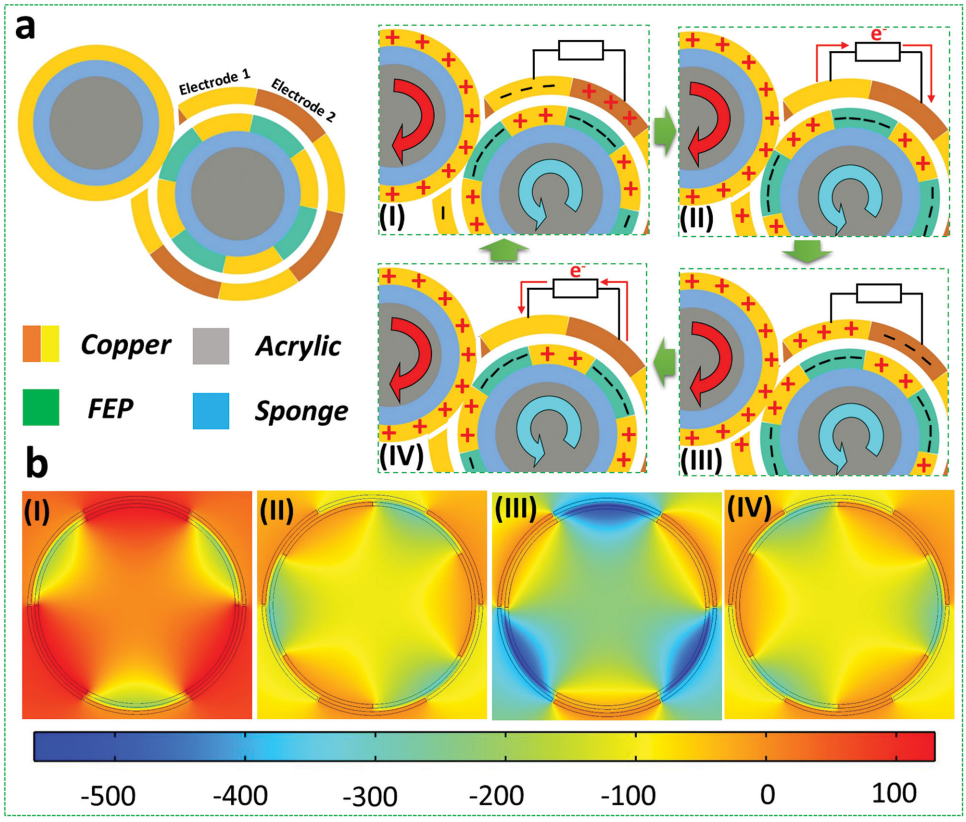

Figure 2. Schematics of the operating principle of the RF-TENG unit. a) Scheme of the working mechanism of the RF-TENG unit for harvesting mechanical rolling energy. b) Numerical calculations of the potential distribution across the electrodes of the RF-TENG at each step (I–IV), as evaluated by COMSOL.

cut-open acrylic tubes, which constituted the stator. Photographs of the as-fabricated electrodes of the rotor and the stator are shown in Figure S1a and b, respectively, in the Supporting Information. Employing a driving system with a gear and a bearing connected to the shaft, the RF-TENG unit can be easily driven by any rotating motion. Figure 1b shows a photograph of a connected shaft/rotor that were linked by gears. A mechanical gear (left-hand) and a bearing (right-hand) are also shown as the inset. Based on the concept mentioned above, several RF-TENG units were integrated into one RF-TENG device to obtain an optimized performance for its practical application in a self-powered system, as shown in Figure 1c. The demonstration of the rolling motion of four rotors, which were connected by gears and then driven by a rotating shaft in the RF-TENG device is shown in the Supporting Information, Movie 1. Moreover, to increase the surface charge density incurred from contact electrification and further enhance the output performance of the RF-TENG, a high surface area was achieved by covering the FEP film with a nanowires array structure using inductively coupled plasma (ICP) reactive-ion etching. A scanning electron microscopy (SEM) image of the FEP film with the nanowires array structure is shown in Figure 1d, which indicates an average nanowire diameter and length of 100 nm and 250 nm, respectively.

The working mechanism of the RF-TENG for generating electricity is based on the coupling effect of contact electrification and electrostatic induction,[11,12] which can be explained in four consecutive steps in a full rotation cycle, as illustrated in **Figure 2**a. Here, electrode 1 and electrode 2 are defined as the individual copper interdigitated electrode on the surface of a stator. First of all, before the rotator starts to spin, no triboelectric charges were generated, as is shown in the left-hand side of Figure 2a. After the rotator starts to drive the rotation of the shaft, a rolling friction occurs at the interface between the Cu-foil-coated shaft and the FEP coated rotor. An equal amount of negative and positive charges will be generated respectively on the FEP parts and the Cu parts due to the difference in electron affinity between them.[6f] At the same time, according to the principle of charge conservation, a redistribution of the positive charges on the Cu shaft and the Cu gratings on the rotor will spontaneously occur due to the intimate contact between the shaft and the rotor. Subsequently, owing to electrostatic induction, the electric field distribution of the negative charges on the FEP film will induce a potential difference between electrode 1 and 2 in the open-circuit condition, which drives electrons to transferring from electrode 2 to 1 through an external load (Step I). When the rotor starts to spin counter clockwise, the negatively charged FEP in the rotor gradually moves away from its intermediate position between electrode 1 and electrode 2 (Step II). In this process, the open-circuit potential difference changes with the relative position change of the negatively charged FEP thin film between the two electrodes, and the electrons on electrode 1 will move back to electrode 2 gradually, until the potential difference reaches its

maximum value with opposite sign (Step III). Another intermediate state of the charge distribution of the stator will be built up by further spinning of the rotor (Step IV), the electric potential difference between electrode 2 and electrode 1 will drive the electrons from the outer circuit to the positively charged Cu electrode until the original state (Step I) is attained. Further rotation beyond this state induces a reversal in both the open circuit voltage and short-circuit current because of the periodic structure. The numerical calculations of the potential distribution across the electrodes of the RF-TENG unit is shown in Figure 2b, which corresponds to the four different states in Figure 2a. From the calculations it was found that the revolution of the potential distribution is consistent with the proposed working mechanism. It is worth noting that the rolling friction can effectively avoid the sliding friction between the surfaces of the shaft and the rotor as no relative motion will occur in such structure with coaxial rotation, as is shown in Figure S2 (Supporting Information). Hence, an ultra-robust electric output performance of the RF-TENG unit could be achieved not only to improve the durability of the materials, but also to provide a sustained charge density on the FEP surface of the rotor.

The electric output performance of the RF-TENG was measured by connecting the shaft to a rotation motor with a rotation speed of 1000 rpm. Photographs of the as-fabricated RF-TENG consisting of four individual RF-TENG units connected together by gears, are presented in Figure S3a (Supporting Information). The integrated rotor and stator part of the RF-TENG are also shown in Figure S3b and c, respectively. First of all, the performance of the open-circuit voltage (V_{OC}) and the short-circuit current (I_{SC}) for each RF-TENG unit (named Unit 1 to 4, respectively) were explored and are shown in **Figure 3**a, which revealed that each RF-TENG unit provided a similar electric output, with a V_{OC} of around 650 V and an I_{SC} of about 55 μA, with only very little variation. In Figure 3b, it is shown that an improved I_{SC} for the bundled RF-TENG can be obtained by connecting various numbers of RF-TENG units in parallel. The transferred charge quantity ($\Delta\sigma$) of the RF-TENG with various configurations is also shown in Figure 3c. With increasing unit numbers of RF-TENG, $\Delta\sigma$ also increases. In the case of an RF-TENG device with four RF-TENG units, the electric output in the form of the I_{SC} and $\Delta\sigma$ can respectively reach up to 240 μA and 380 nC, which form roughly a four times enhancement as compared to the single-unit RF-TENG. According to the above results, it may be concluded that the RF-TENG with 4 units with parallel electric connection provides an effective superposition of the electric output from the single units.

One of the advantages of RF-TENGs is that a synchronized rolling motion of each rotor can be fully realized by means of transmission from connected gears and driving by a rotating motor. In such conditions, a phase mismatch of the generated charges for each RF-TENG can be avoided and efficient transferring of the electricity via harvesting of the mechanical rotating energy can be achieved. On the other hand, the V_{OC} value shows no obvious difference between each RF-TENG unit (Unit 1 to 4) nor does its value differ much for the RF-TENG composed of various amounts of RF-TENG units connected in parallel. To be able to use our proposed RF-TENG in practical applications, a full-wave bridge rectifier was employed to convert the generated alternating-current pulses into direct-current signals, as shown in Figure 3d–f. The result of the DC output for the RF-TENG was almost similar to that of the AC one, namely, excellent superposition characteristics were found by adding up the current output through the integration of multiple RF-TENG units. After the device was connected to a rectifier, the I_{SC} and V_{OC} of the RF-TENG with 4 RF-TENG units were as high as 185 μA and 325 V, respectively. Furthermore, based on the above results, further improvements in the electric output of the RF-TENG device could be accomplished by integrating more units into the device.

To further increase the electric output of RF-TENG, several geometric parameters for fabricating each RF-TENG unit, such as the free-standing separation distance and grating numbers, were thoroughly investigated. Our previous work has already provided a systematic study of the influence of the design parameters, including the gap distance and grating number, on the electric output of the RF-TENG, which was performed both theoretically and experimentally.[6f] In this work, the previously found optimized parameters, including the free-standing separation distance of 0.5 mm and grating number of 30, for achieving high performance RF-TENG units were directly adopted without further discussion. On the other hand, the rotation speed is another important factor that could have an impact on the electric output performance of the RF-TENG. The value of I_{SC} under a series of rotation speeds ranging from 300 to 1500 rpm was measured and is displayed in **Figure 4**a. It can clearly be seen that I_{SC} increases with rotation speed, as the output current is the time differentiation of the transferred charges across the external load. Furthermore, it can be concluded that the value of V_{OC} is independent of the rotation speed as no obvious change was observed in the voltage measurement. Moreover, various load resistances ranging from 1 kΩ to 100 MΩ were utilized as the external load to further investigate the output power of the RF-TENG with different configurations of 1, 2, 3, and 4 RF-TENG units (at a rotation rate of 1000 rpm), as displayed in Figure 4b. As a result, the instantaneous peak power was maximized at a load resistance of 20 MΩ, corresponding to a peak power of 50 mW for the RF-TENG with four RF-TENG units. The output enhancement trend by increasing the amount of units implies that further improvement of the electric output of the bundled RF-TENG can be realized by integrating more RF-TENG units. On the other hand, the device robustness is another important factor that should be considered. It is worth noting that reliability is one of the important features to be met by our proposed RF-TENG device, which would be primarily represented by its output stability and mechanical durability. To examine these factors, the output stability was measured after long-term continuous rotation and is shown in Figure 4c. Less than ±0.5% of electric output fluctuation was observed after 1.5 million cycles (fixed rotation speed of 500 rpm for 2 days). The mechanical durability of our RF-TENG was also investigated and evaluated by comparing the state of the FEP surface before and after continuous working for 1.5 million cycles, as shown in the inset of Figure 4c. As shown by the SEM image, no significant distortion or serious damage of the FEP nanowire structure surface was observed

Adv. Funct. Mater. 2015,
DOI: 10.1002/adfm.201504396

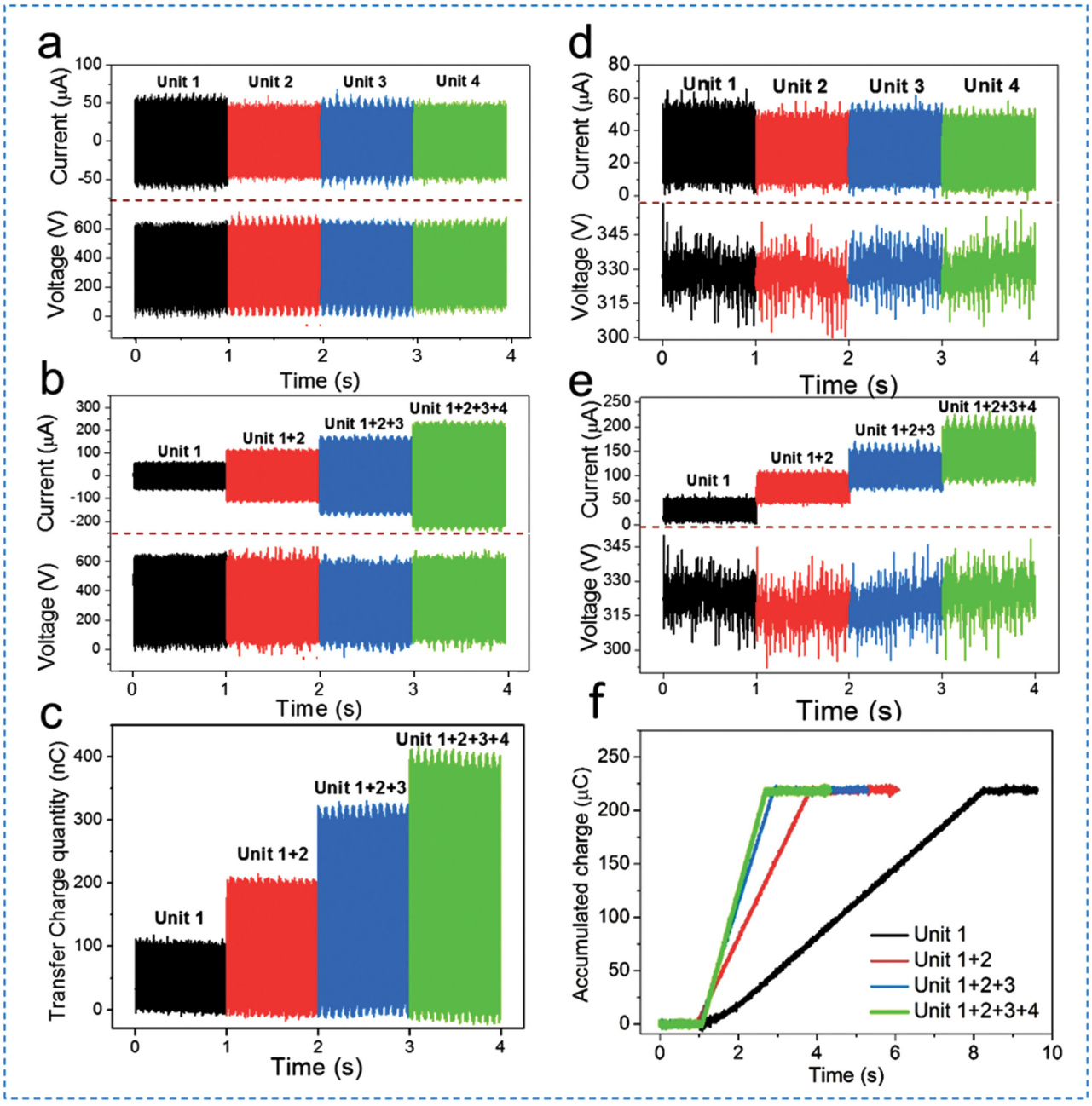

Figure 3. Electric output performance of the RF-TENG with different numbers of RF-TENG units at a rotation speed of 1000 rpm. a) Open-circuit voltage (V_{OC}) and short-circuit current (I_{SC}) for each RF-TENG unit. b) V_{OC} and I_{SC} for RF-TENG devices with different configurations of 1, 2, 3, and 4 RF-TENG units. c) Transfer-charge quantity for RF-TENG devices with 1, 2, 3, and 4 RF-TENG units. d) Performance of the rectified V_{OC} and the rectified I_{SC} for each RF-TENG unit. e) Performance of the rectified V_{OC} and the rectified I_{SC} for RF-TENG devices with different configurations of 1, 2, 3, and 4 RF-TENG units. f) Accumulated charge for RF-TENG devices with different configurations of 1, 2, 3, and 4 RF-TENG units.

after continuous rotation. This can mainly be attributed to the fact that rolling friction effectively minimizes abrasion of the materials. The outstanding robustness of the RF-TENG can be attributed to several factors, which were elucidated in detail. The continuous charge replenishment was achieved by a shaft rolling friction. The mechanical durability could be enhanced by utilizing a rolling friction contact mode to minimize the contacting damage. Moreover, relative slipping and irregular rolling could be avoided at the interface between the shaft and the rotor by incorporating a triboelectric layer with appropriate gearing. By connecting a conventional rotator, the electric output power of the RF-TENG could be used to simultaneously power 10 spot LED lights connected in parallel (Figure 4d, and Supporting Information, Movie 2).

Our RF-TENG provides a promising structure as a generator to harvest different types of mechanical energy from the natural environment. It should be noted that TENGs have been proposed before for providing more output power and other

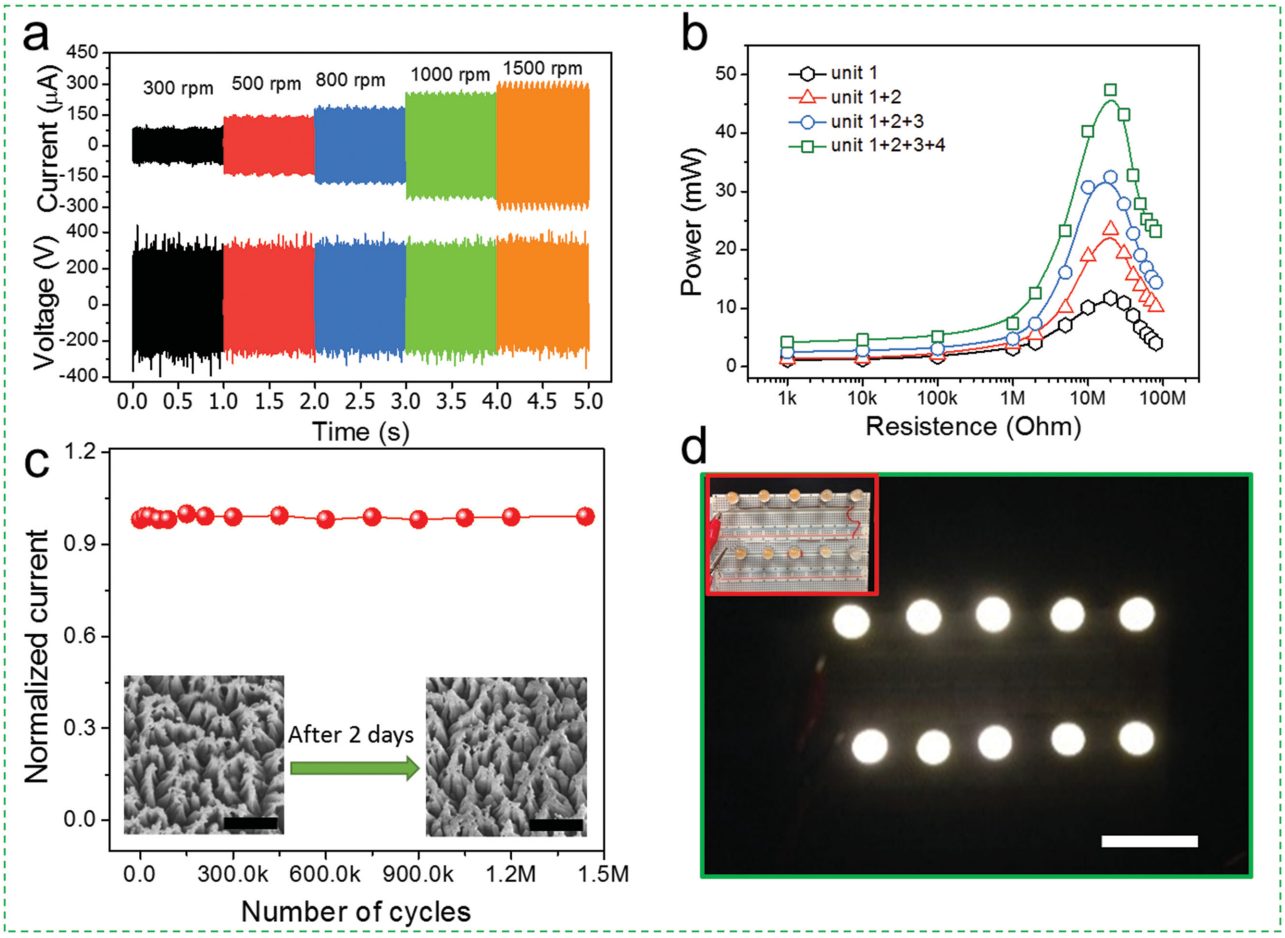

Figure 4. Demonstrations of the RF-TENG as a practical power source. a) Electric output characterization of an RF-TENG with four RF-TENG units under various rotating speeds. b) Dependence of the output current and peak power of the RF-TENG with different configurations of 1, 2, 3, and 4 RF-TENG units on the resistance of the external load, indicating that the maximum power output was obtained at 20 MΩ. The results were obtained at a fixed rotating speed of 1000 rpm. c) Robustness test of the RF-TENG. No obvious normalized current decay was found after 1.5 M rotation cycles (at a fixed rotation speed of 500 rpm for 2 days). Inset: SEM images (scale bar is 1 μm) showing that no significant distortion or serious damage was observed on the FEP nanowire structure surface after continuous rotation. d) Photograph of 10 spot lights that were directly powered by the RF-TENG under a rotating speed of 1500 rpm. The scale bar is 2 cm.

advantages as compared to conventional electromagnetic generators (EMGs),[7] which implies that TENGs can be used as potential power generators to replace some self-powered systems that are driven by traditional EMGs. In practical applications, for example, RF-TENGs can be easily coupled with a waterwheel or a water turbine via a coaxial design. A photograph of a water wheel that was used to drive our RF-TENG is shown in **Figure 5**a. As shown in the Supporting Information (Movie 3), the energy of flowing water can be effectively transformed by a water wheel into a rotary motion of the shaft to drive the RF-TENG device.

Furthermore, a self-powered electrochemical copper collecting system was achieved by incorporating with an electrochemical cell and a water-driven RF-TENG. To simulate our proposed system, a two-electrode electrochemical cell (Figure 5b) that consists of a graphite rod as the anode and a copper plate as the cathode was utilized and $CuSO_4$ aqueous solution (2.5 g L^{-1}) was used as the electrolyte to simulate wastewater containing Cu^{2+} ions. According to the electroplating effect, the reduction of the Cu^{2+} ions occurs on the surface of the cathode and can be written as:[13]

$$Cu^{2+} + 2e^- \rightarrow Cu \quad E_0 = 0.3402\ \text{V (vs NHE)} \tag{1}$$

A DC power supply with steady output potential is indispensable for driving this reaction efficiently and smoothly. To realize the above requirement, the output of the RF-TENG was integrated with a conventional transformer and a power-management circuit composed of a full-wave bridge rectifier, a voltage regulator, and capacitors, as shown in the circuit diagram of Figure 5c. With the help of the power transformer, the output current of the RF-TENG was effectively boosted from 250 μA to 8 mA, whereas the voltage was reduced from 650 V to 16 V, which means that the transformed efficiency was around 80% (Figure 5d). The transformed output could still produce a high enough potential to initiate the electrochemical reaction, but the speed of the reaction was greatly improved due to the drastic enhancement in the current. Therefore, as

Adv. Funct. Mater. **2015**,
DOI: 10.1002/adfm.201504396

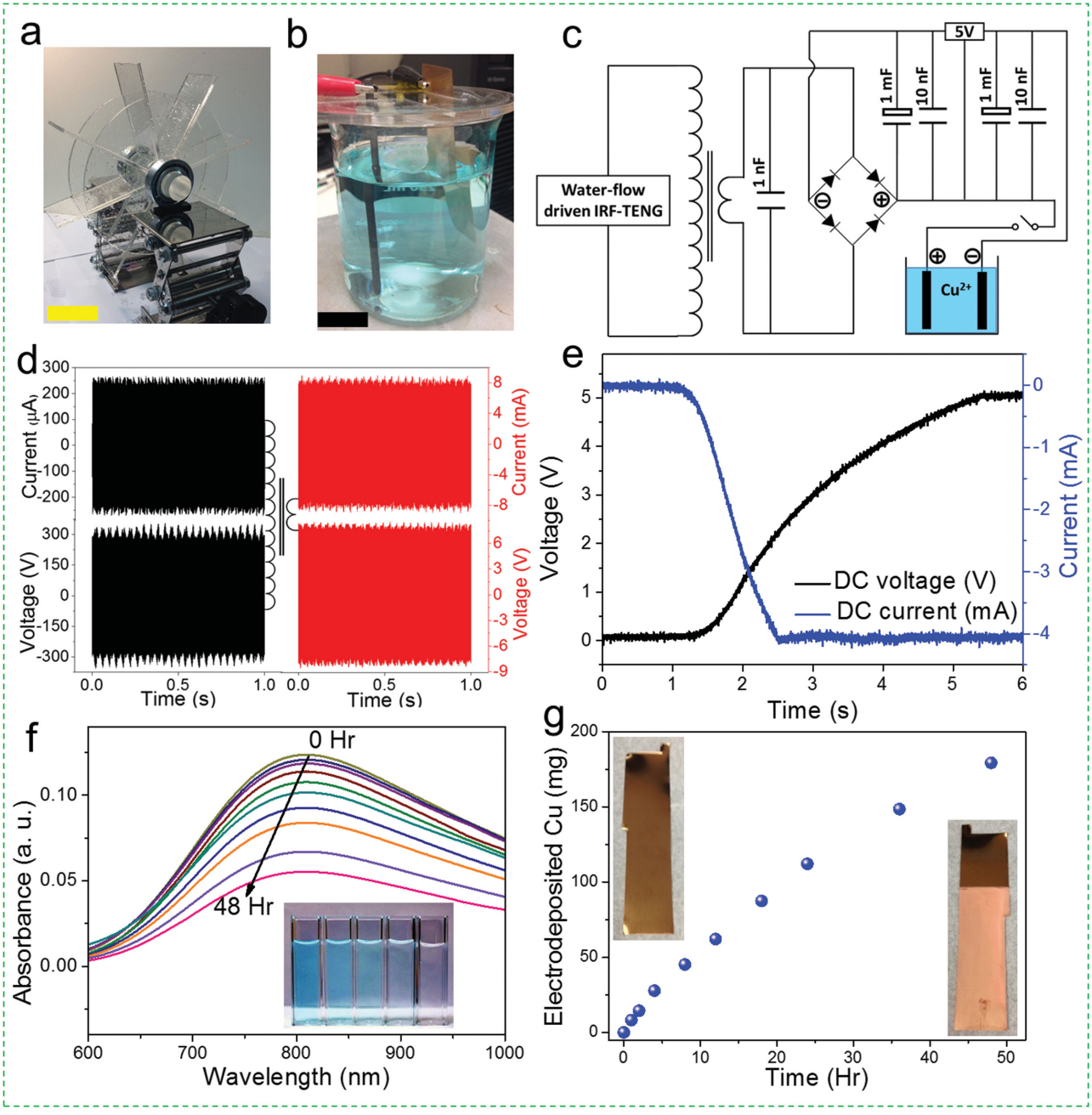

Figure 5. Demonstrations of the RF-TENG for harvesting hydroenergy from flowing water and its practical applications in a self-powered electrochemical recovery system for collecting Cu^{2+} ions. a) Photograph of the water wheel used for driving the RF-TENG by harvesting the energy of the flowing water. The scale bar is 5 cm. b) Photograph of the two-electrode electrochemical system, consisting of a graphite rod anode and a copper plate cathode; $CuSO_4$ aqua solution (2.5 g L^{-1}) was used as the electrolyte. The scale bar is 2 cm. c) Circuit diagram of a self-powered electrochemical recovery system for collecting Cu^{2+} ions, composed of the stable power-supply system that integrated a water-driven RF-TENG, a power management circuit, and a two-electrode electrochemical cell. d) V_{OC} and I_{SC} for the water-driven RF-TENG (left hand side) and corresponding electric performance by applying a transformer (right hand side). e) Stable output DC voltage (5 V) and current (4 mA) obtained by the power-supplying system, which consisted of a water-driven RF-TENG and a power management circuit. f) UV–vis absorption spectra of the Cu^{2+} ions in the wastewater obtained at different duration times. The inset shows pictures of the Cu^{2+} solution at different times to depict the change in color of the Cu^{2+} solution. g) Corresponding weight of electrodeposited Cu as a function of operating time. The inset shows the photograph of the fresh Cu electrode (left) and after Cu collection (right).

shown in Figure 5e, a stable DC electric output of 5 V and 4 mA was delivered by incorporating it with another power management circuit. Figure 5f shows the real-time monitoring of the UV–vis absorption spectra of the Cu^{2+} ions in the wastewater obtained at different times. With increasing time of the electrochemical collection process, the characteristic absorption peak intensity of the Cu^{2+} ions in the wastewater decreased evidently, indicating the effectiveness of the

self-powered electrochemical deposition. Also, pictures of the wastewater containing Cu^{2+} ions at different times are also presented in the inset of Figure 5f to depict the change in color of the Cu^{2+} solution. The recovery rate of Cu^{2+} ions could be further estimated by utilizing a calibration curve (Figure S4, Supporting Information), as shown in Figure 5g. As expected, the deposited amount of copper increased as time passed by and then reached a saturation point after 48 h. A photograph of the original copper plate (left) and one of the plate deposited with copper (right) are attached as insets in Figure 5g. An energy-conversion efficiency of up to 80% (practical collection weight: 180 mg; theoretical collection weight: 227.5 mg) for collecting Cu^{2+} ions from the wastewater was achieved by utilizing our proposed self-powered electrochemical collection system. Our proposed RF-TENG can be easily installed in current wastewater treatment systems as a power supplier for harvesting flowing-water energy and further driving the electrowinning process (as shown in Figure S5, Supporting Information). Moreover, several other electrochemical processes in practical wastewater electrochemical treatments, such as electrocoagulation, electroflotation, electrochemical degradation, and electrochemical advanced oxidation processes, could also be driven by our proposed self-powered electrochemical processor.

3. Conclusion

We have developed a RF-TENG device that utilizes integrated cylindrical surfaces through the conjunction of rolling contact-electrification and free-standing electrostatic induction as a sustainable power supply. The concept of a self-powered electrochemical recovery system for collecting Cu metal was realized by integrating a RF-TENG and an electrochemical cell. The RF-TENG used the energy of flowing water to transform into a rotating energy that delivered an output current of up to 280 μA, corresponding to an effective power of 50 mW. Even after continuous rotation of more than 1.5 million cycles for 2 days no observable electric output degradation was found. This superior device reliability and high-output performance was used to accomplish the RF-TENG as a continuous power system for harvesting flowing water energy to drive the electrodeposition reaction and recovery of Cu from wastewater. A collection efficiency of up to 80% of the Cu^{2+} ions in the wastewater was achieved by utilizing our proposed self-powered electrochemical collection system. This research presents a substantial advancement in the practical applications of triboelectric-based nanogenerators and self-powered electrochemical systems, which will initiate promising improvements in related electrochemical fields.

4. Experimental Section

Fabrication of FEP Film with Nanowires Array Structure: The fluorinated ethylene propylene (FEP) film with nanowire array structure was fabricated by inductively coupled plasma (ICP) reactive-ion etching. Briefly, a 50 μm thick FEP thin film (American Durafilm) was first cleaned with methanol, isopropyl alcohol, and deionized water sequentially, and then blown dry with nitrogen gas. After that, a uniform Au thin layer was deposited on the surface of the FEP thin film by sputtering (Unifilm Sputter) as the mask for creating the nanowire array structure via an ICP etching process. Subsequently, Ar, O_2, and CF_4 gases were introduced into the ICP chamber at a flow rate of 10, 15, and 30 sccm, respectively. The FEP film was etched (plasma-ion acceleration = 100 W) for 10 min to obtain the nanowire array structure on its surface.

Fabrication of a Rotor and a Stator: For fabricating a rotor for the RF-TENG, a piece of the as-fabricated FEP film (10 cm × 8 cm) was coated with copper strings (film thickness ca. 1 μm) by physical vapor deposition (model: PVD 75, Kurt J. Lesker). Subsequently, two pieces of copper-coated FEPs (surface area of triboelectrification layer = 160 cm^2) were attached to the surface of the acrylic rod (D = 25.4 cm, L = 30.5 cm), which was covered with a soft sponge foam (firmness = 4–8 psi). The sponge foam not only acted as a buffer layer to enhance the intimate contact between the copper rod and the FEP film, but also avoid the relative slipping between the surface of the FEP and the copper rod, which enhanced its mechanical durability. On the other hand, a Kapton film with deposited copper electrodes, which were complementarily patterned and interspaced by fine trenches, was prepared and then coated on the inner surface of the cut-open acrylic tubes (cut width: 12 mm, inner diameter: 29 mm) as the stator for the RF-TENG.

Characterization and Electric Measurements of the RF-TENG: The morphology of the FEP film with nanowire array structure was characterized by field-emission scanning electron microscopy (FE-SEM, SU8010, Hitachi). For the electric output measurement of the RF-TENG, a programmable electrometer (model: 6514, Keithley) was used for recording the output voltage and current.

Electrochemical Cell for Collecting Copper Ions: A two-electrode electrochemical cell was used as the Cu^{2+} collecting system. Furthermore, a graphite rod and copper plate (99.9%, Sigma-Aldrich) acted as the anode and cathode, respectively. A copper(II) sulfate ($CuSO_4{\cdot}5H_2O$, ≈98–102%, Alfa Aesar) aqua based solution with a concentration of 2.5 g L^{-1} was utilized as the electrolyte. The absorbance spectra of the Cu^{2+} solution were monitored by UV–vis spectrophotometry (V-630JASCO). At various operating times (0–48 h), the concentration of Cu^{2+} was calculated and recorded accurately using a calibration curve.

Supporting Information

Supporting Information is available from the Wiley Online Library or from the author.

Acknowledgements

M.H.Y. and H.G. contributed equally to this work. M.H.Y. thanks the support from the Ministry of Science and Technology, Taiwan (MOST 103–2917-I-564–070). H.G. acknowledges the fellowship from the China Scholarship Council (CSC).

Received: October 14, 2015
Revised: November 16, 2015
Published online:

[1] S. Babel, T. A. Kurniawan, *J. Hazardous Mater.* **2003**, *97*, 219.
[2] F. Fu, Q. Wang, *J. Environ. Manage.* **2011**, *92*, 407.
[3] G. Chen, *Sep. Purif. Technol.* **2004**, *38*, 11.
[4] a) Z. L. Wang, *Adv. Mater.* **2012**, *24*, 280; b) Z. L. Wang, *Adv. Funct. Mater.* **2008**, *18*, 3553; c) Z. L. Wang, *Sci. Am.* **2008**, *298*, 82; d) Z. L. Wang, W. Wu, *Angew. Chem. Int. Ed.* **2012**, *51*, 11700; e) G. T. Hwang, H. Park, J. H. Lee, S. Oh, K. I. Park, M. Byun, H. Park, G. Ahn, C. K. Jeong, K. No, H. Kwon, S. G. Lee, B. Joung, K. J. Lee, *Adv. Mater.* **2014**, *26*, 4880; f) R. Zhang, S. Wang,

M.-H. Yeh, C. Pan, L. Lin, R. Yu, Y. Zhang, L. Zheng, Z. Jiao, Z. L. Wang, *Adv. Mater.* **2015**, *27*, 6482.

[5] a) S. Wang, L. Lin, Z. L. Wang, *Nano Energy* **2015**, *11*, 436; b) Z. L. Wang, *Faraday Discuss.* **2014**, *176*, 447; c) Z. L. Wang, *ACS Nano* **2013**, *7*, 9533; d) G. Zhu, B. Peng, J. Chen, Q. Jing, Z. Lin Wang, *Nano Energy* **2015**, *14*, 126.

[6] a) L. Lin, S. Wang, Y. Xie, Q. Jing, S. Niu, Y. Hu, Z. L. Wang, *Nano Lett.* **2013**, *13*, 2916; b) G. Zhu, P. Bai, J. Chen, Z. Lin Wang, *Nano Energy* **2013**, *2*, 688; c) S. Wang, Y. Xie, S. Niu, L. Lin, C. Liu, Y. S. Zhou, Z. L. Wang, *Adv. Mater.* **2014**, *26*, 6720; d) Y. Xie, S. Wang, S. Niu, L. Lin, Q. Jing, Y. Su, Z. Wu, Z. L. Wang, *Nano Energy* **2014**, *6*, 129; e) G. Zhu, J. Chen, T. Zhang, Q. Jing, Z. L. Wang, *Nat. Commun.* **2014**, *5*, 3426; f) H. Guo, J. Chen, M. H. Yeh, X. Fan, Z. Wen, Z. Li, C. Hu, Z. L. Wang, *ACS Nano* **2015**, *9*, 5577; g) H. Guo, J. Chen, Q. Leng, Y. Xi, M. Wang, X. He, C. Hu, *Nano Energy* **2015**, *12*, 626; h) H. Guo, Q. Leng, X. He, M. Wang, J. Chen, C. Hu, Y. Xi, *Adv. Energy Mater.* **2015**, *5*, 1400790; i) C. K. Jeong, K. M. Baek, S. Niu, T. W. Nam, Y. H. Hur, D. Y. Park, G. T. Hwang, M. Byun, Z. L. Wang, Y. S. Jung, K. J. Lee, *Nano Lett.* **2014**, *14*, 7031.

[7] C. Zhang, W. Tang, C. Han, F. Fan, Z. L. Wang, *Adv. Mater.* **2014**, *26*, 3580.

[8] a) S. Wang, L. Lin, Z. L. Wang, *Nano Lett.* **2012**, *12*, 6339; b) W. Tang, B. Meng, H. X. Zhang, *Nano Energy* **2013**, *2*, 1164.

[9] a) M. H. Yeh, L. Lin, P. K. Yang, Z. L. Wang, *ACS Nano* **2015**, *9*, 4757; b) W. Tang, Y. Han, C. B. Han, C. Z. Gao, X. Cao, Z. L. Wang, *Adv. Mater.* **2015**, *27*, 272.

[10] a) Z. Li, J. Chen, J. Yang, Y. Su, X. Fan, Y. Wu, C. Yu, Z. L. Wang, *Energy Environ. Sci.* **2015**, *8*, 887; b) Z. H. Lin, G. Zhu, Y. S. Zhou, Y. Yang, P. Bai, J. Chen, Z. L. Wang, *Angew. Chem. Int. Ed.* **2013**, *52*, 5065; c) Z. Wen, J. Chen, M. H. Yeh, H. Guo, Z. Li, X. Fan, T. Zhang, L. Zhu, Z. Lin Wang, *Nano Energy* **2015**, *16*, 38; d) X. Li, M. H. Yeh, Z. H. Lin, H. Guo, P.-K. Yang, J. Wang, S. Wang, R. Yu, T. Zhang, Z. L. Wang, *ACS Nano* **2015**, *9*, 11056.

[11] L. Lin, Y. Xie, S. Niu, S. Wang, P. K. Yang, Z. L. Wang, *ACS Nano* **2015**, *9*, 922.

[12] F. R. Fan, Z. Q. Tian, Z. Lin Wang, *Nano Energy* **2012**, *1*, 328.

[13] M. Hunsom, K. Pruksathorn, S. Damronglerd, H. Vergnes, P. Duverneuil, *Water Res.* **2005**, *39*, 610.